Supporting Information Available

Phenylenediamine-Based FeN_x/C Catalyst with High Activity for Oxygen Reduction in Acid Medium and Its Active-Site Probing

Qiang Wang,[†] Zhi-You Zhou,*[,†] Yu-Jiao Lai,[†] Yong You,[‡] Jian-Guo Liu,[‡] Xia-Ling Wu,[†] Ephrem Terefe,[†] Chi Chen,[†,§] Lin Song,[†] Muhammad Rauf,[†] Na Tian[†] and Shi-Gang Sun*[,†]

[†] *State Key Laboratory of Physical Chemistry of Solid Surfaces, Department of Chemistry, College of Chemistry and Chemical Engineering, Xiamen University, Xiamen 361005, China.*

‡ *Eco-materials and Renewable Energy Research Center, Department of Materials Science and Engineering, and National Laboratory of Solid State Microstructures, Nanjing University, Nanjing 210093, China.*

§ *State Key Laboratory of Chemical Engineering, East China University of Science and Technology, Shanghai 200237, China.*

Email: zhouzy@xmu.edu.cn; sgsun@xmu.edu.cn

1. Materials and methods

4-Aminobenzenesulfonic acid (98.0+%, Alfa Aesar), Sulfuric acid (suprapur 96.0%, Merck), Selenium dioxide (SeO_2, 99.99%, Aladdin), Sodium tellurite (Na_2TeO_3, 99.9%, Aladdin), Ketjenblack EC600J (KJ600, Akzo Nobel), Nafion (D520, 5%, Dupont) were used as received. Meta-phenylenediamine (*m*-PDA, 98+%), iron powder reduced (98%), ferric chloride ($FeCl_3$, 99.0%), ammonium persulfate ($(NH_4)_2S_2O_8$, 98%), sodium nitrite ($NaNO_2$, 99.0%), sodium hydroxide (NaOH, G.R. 98.0%), hydrochloric acid (HCl, 36%-38%), sodium thiocyanate (NaSCN, 99.5%), sodium chloride (NaCl, 99.5%), sodium fluoride (NaF, 98.0%), and sodium bromide (NaBr, 99.0%) were purchased from China Medicine Shanghai Chemical Reagent Corp. High purity Ar (99.999%), O_2 (99.998%) and N_2 (99.99%) were purchased from Linde.

Electrochemical studies were carried out in a standard three-electrode cell connected to a CHI-760D bipotentiostat (CH Instruments, Inc., China). Counter electrode was a thin graphite plate (5×2 cm) and reference electrode was a reversible hydrogen electrode (RHE). Working electrode was a rotating ring-disk electrode (RRDE) with Pt ring and glassy carbon disk (GC, ϕ = 5.61 mm) purchased from Pine Instrument, Inc. Rotating rate was fixed at 900 rpm. Electrochemical cell was placed in 30 ºC water bath.

X-ray photoelectron spectroscopy (XPS) was carried out using a Qtac-100 LEISS-XPS instrument. Ar adsorption/desorption isotherm was tested by a Micromeritics ASAP 2020 system (USA). The specific surface area was determined through Brunauer-Emmett-Teller (BET) method. X-ray diffraction (XRD) was performed on Rigaku Ultima IV with Cu Kα radiation. TEM was measured on JEM-2100 at 200 kV. The particle size distribution of carbon black in solution was obtained using a laser granulometer (CILAS-1604L) with a laser wavelength of 830 nm and power of 3 mW.

2. Preparation of PmPDA-FeNx/C catalyst

The preparation process of PmPDA-FeN_x/C is illustrated in Figure S1.

To improve the hydrophilicity, the KJ600 carbon black was grafted with sulfophenyl group through reduction of diazonium salt.[S1] The sulfophenyl diazonium salt was synthesized through 4-Aminobenzenesulfonic acid (8.2 mmol), $NaNO_2$ (8.2 mmol), and 1 M HCl (18 mL) in 3 °C cooling bath. The obtained diazonium salt and reduced Fe powder were poured into the carbon black (2 g) suspension. The reaction mixture was stirred overnight to graft sulfophenyl group onto carbon surface. The obtained carbon black was denoted as $KJ600_{GF}$.

The above $KJ600_{GF}$ suspension in 5 °C was mixed with *m*-PDA (15 g) and concentrated HCl (36%, 50 mL). To this suspension, pre-cooled $(NH_4)_2S_2O_8$ (2 M, 140 mL) and $FeCl_3$ (1 M, 40 mL) solution were added drop by drop to oxidize m-PDA into poly-m-PDA (P*m*PDA) for coating on grafted carbon black. The suspension was filtered and water washed to remove inorganic salts. The Fe salt was also completely removed in this step, and the residual Fe was below 0.1 *wt*% as determined by Inductively Coupled Plasma Optical Emission Spectrometer (ICP-OES). The acquired powder was denoted as P*m*PDA-$KJ600_{GF}$.

The dry powder of P*m*PDA-$KJ600_{GF}$ (3.6 g) was mixed with $FeCl_3$ (1 M, 9 mL) solution and 100 mL water. Then, the solvent was removed through rotary evaporator and further dried in oven for 12 h at 80 °C. The resulting powder was subjected to the 1st heat treatment (HT1) at temperatures ranging from 600 to 1000°C in high-purity Argon atmosphere for 1 h. The pyrolyzed sample was then acid leached (AL) in 1 M HCl solution at 80 °C for 8 h followed by centrifugation and washing with deionized water. This step was performed to removing ORR inactive and unstable compounds (e.g., Fe_3C and FeS) from the catalyst. Finally, the obtained powder was heat treated for the 2nd time (HT2) at the same temperature as HT1 for 3 h. The final catalyst was denoted as P*m*PDA-FeN_x/C.

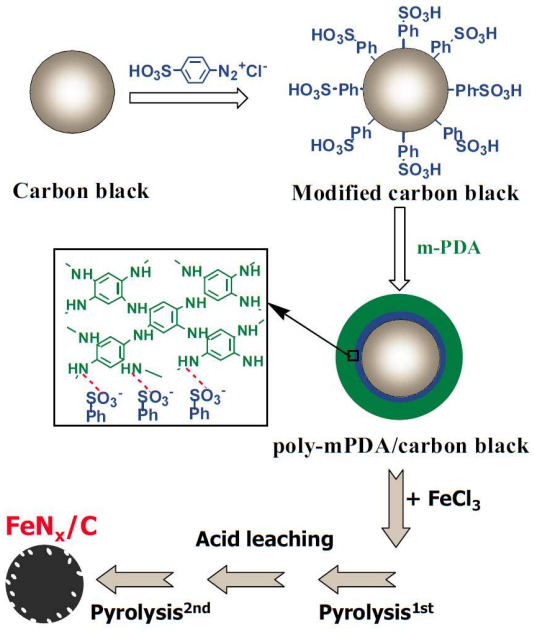

Figure S1. Illustration of synthesizing PmPDA-FeN_x/C catalyst

3. ORR performance test

To deposit the catalyst onto the GC disk electrode, 6.0 mg of catalyst sample was ultrasonically dispersed in 0.5 mL water, 0.5 mL ethanol, and 50 μL 5 *wt*% Nafion solution for 1 hour to form a uniform catalyst ink. Then, 25 μL of the ink was dropped onto the GC disk of the RRDE, resulting in catalyst loading of 600 μg cm^{-2}. To obtain a uniform catalyst layer, the RRDE was slowly rotated at a rate of about 300 rpm during the drying process. The electrolyte was 0.1 M H_2SO_4 and was bubbled with high pure oxygen at 40 sccm. The GC disk electrode was subjected to potential cycling between 1.0 to 0.2 V (RHE) at a scan rate of 10 mV s^{-1} with rotating rate of 900 rpm. Solution ohmic drop (i.e., iR drop) was compensated. The background capacitive current was recorded in the same potential range and scan rate, but in N_2-saturated electrolyte. The current recorded in O_2-saturated solution was corrected for the background current to yield net ORR current of the tested catalyst.

The kinetic current (i_k) for the ORR can be derived from the experimental data using the Koutecky-Levich equation (Eq. 1) for rotating disk electrodes:

$$\frac{1}{i} = \frac{1}{i_L} + \frac{1}{i_k} \qquad (1)$$

where i and i_L are the measured current and diffusion limiting current, respectively. The mass activity (j_m) is calculated via the normalization of i_k with the catalyst mass.

To detect H_2O_2 yield, the ring potential was set to 1.2 V (RHE) to oxidize the H_2O_2 transferred from GC disk electrode. The H_2O_2 yield was calculated by following equation (Eq. 2):

$$\mathrm{H_2O_2}(\%) = 200 \times \frac{I_R / N_0}{(I_R / N_0) + I_D} \qquad (2)$$

Where, I_D and I_R are the disk and ring currents, respectively, and N_0 is the ring collection efficiency. The N_0 was determined to be 0.386 ± 0.002 in a solution of 5 mM $K_4Fe(CN)_6$ + 1 M $Sr(NO_3)_2$.

During the study of the effects of small molecules and inorganic ions, polarization curves were firstly recorded in O_2 and N_2-saturated 0.1 M H_2SO_4 (blank) solution, and then the bubbling gas was switched to mixture gas (e.g., O_2 + CO), or inorganic salts (e.g., NaCl) were added into the solution.

4. Fuel cell test

The cathode catalyst was P*m*PDA-FeN_x/C with a loading of 4 mg cm^{-2}. To enhance protonic conductivity, 60 *wt*% of Nafion content in cathode catalyst layer was used. The anode catalyst was 60 *wt*% Pt/C from Johnson Matthey with a loading of 0.5 mg Pt cm^{-2}, and the Nafion content in anodic catalyst layer was 30 *wt*%. The catalyst layer in the anode and the cathode was brushed on the gas diffusion layer (Sunrise Power Inc. China) based on Toray 060 carbon paper. Then, the MEA was prepared by hot-pressing the electrodes and Nafion 211 membrane with an active area of 2.0 cm^2. Fuel cell polarization curve was tested at 80 ^oC on a fuel cell test system (Model 850e, Scribner Associates Inc.). H_2 and O_2 flow rates were 300 mL min^{-1} at 100% RH, and no back pressure was applied (i.e., the O_2 and H_2 partial pressure was about 0.53 bar since the saturation water vapor pressure at 80 ^oC is ca 0.47 bar). The polarization curve was recorded by scanning the cell voltage from open circuit potential (OCP) down to 0.25 V at a scan rate of 0.5 mV s^{-1}.

5. Particle distribution of carbon black in solution

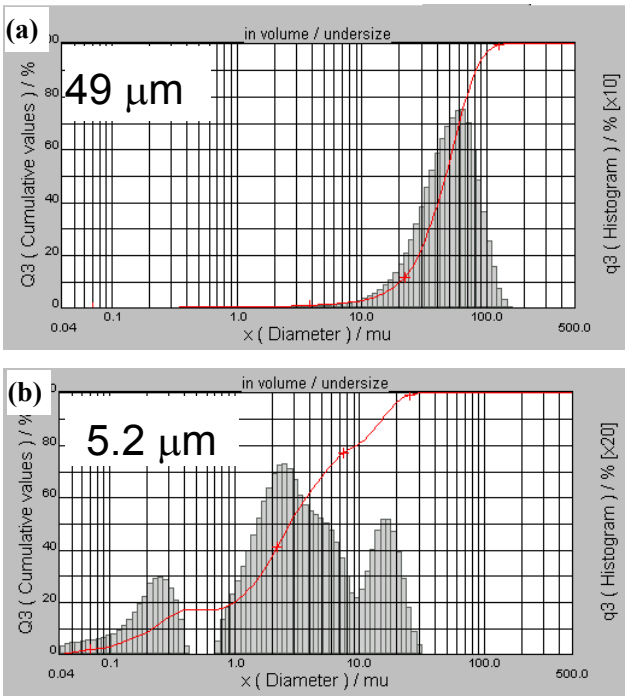

Figure S2. Laser diffraction particle size analysis of carbon black in solution. (**a**) pristine KJ600; (**b**) KJ600-Ph-SO_3H.

The surface modification of sulfophenyl (-Ph-SO_3H) group on carbon black can greatly improve the dispersion in water solution. Laser diffraction particle size analysis indicates that the average diameter of carbon agglomerates in solution decreasing from 49 μm (Figure S2a) to 5.2 μm (Figure S2b) after surface modification.

6. XRD characterization and ORR performance of the samples at different pyrolysis process

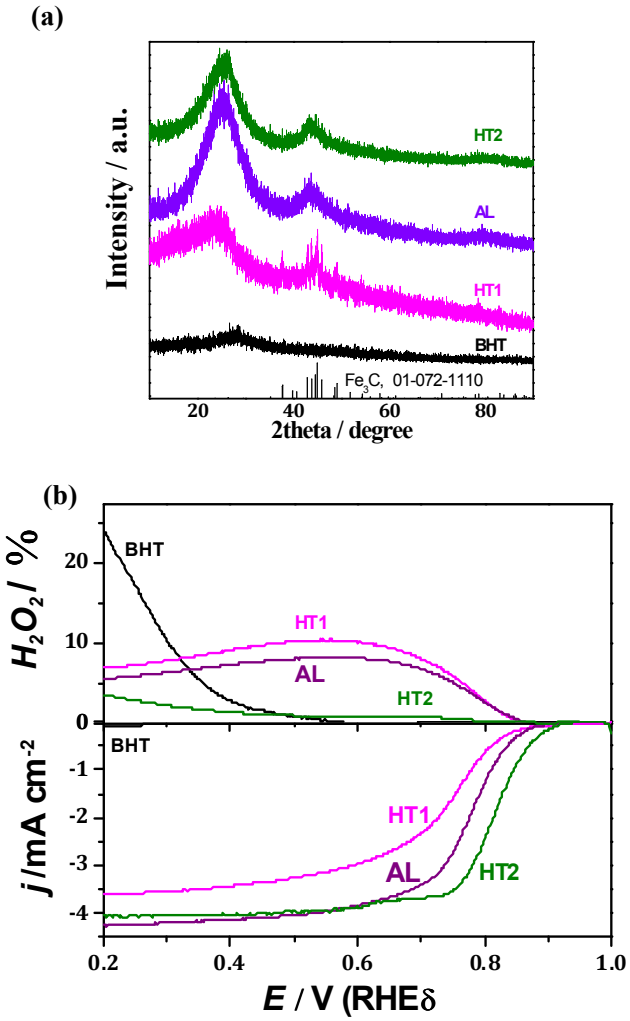

Figure S3 XRD (**a**) and ORR performance (**b**) of P*m*PDA-FeN$_x$/C (950 ^{o}C) catalyst at different synthesis steps. Crystalline Fe_3C (ICDD PDF2 File #01-072-1110) can be observed at HT1 sample. BHT: before heat treatment; HT1: first heat treatment; AL: acid leaching; HT2: Second heat treatment.

Figure S3a shows the X-ray diffraction (XRD) patterns of the P*m*PDA-FeN$_x$/C (950 ^{o}C) catalyst at different synthesis steps. Before heat treatment (**BHT**), only a weak and broad peak at 28.0^{o} can be observed, indicating the sample is amorphous phase and $FeCl_3$ is well dispersed. After the first heat treatment (**HT1**) at 950 °C in Argon atmosphere for 1 h, some crystalline phases appear, such as Fe_3C, sometimes FeS and metallic Fe also appear. These crystalline species can be removed completely after acid leaching (**AL**). After the second heat treatment (**HT2**) at 950 °C for 3 h, no considerable change can be observed in XRD pattern, and two broad peaks centred at 25.3^{o} and 43.7^{o} come from graphite.

Figure S3b shows the ORR performance of corresponding samples. Before heat treatment, ORR activity is very low. After HT1, the activity increases greatly, and further increases after AL and HT2. The yield of H_2O_2 shows the opposite trend.

7. TEM and Ar adsorption isotherm characterization

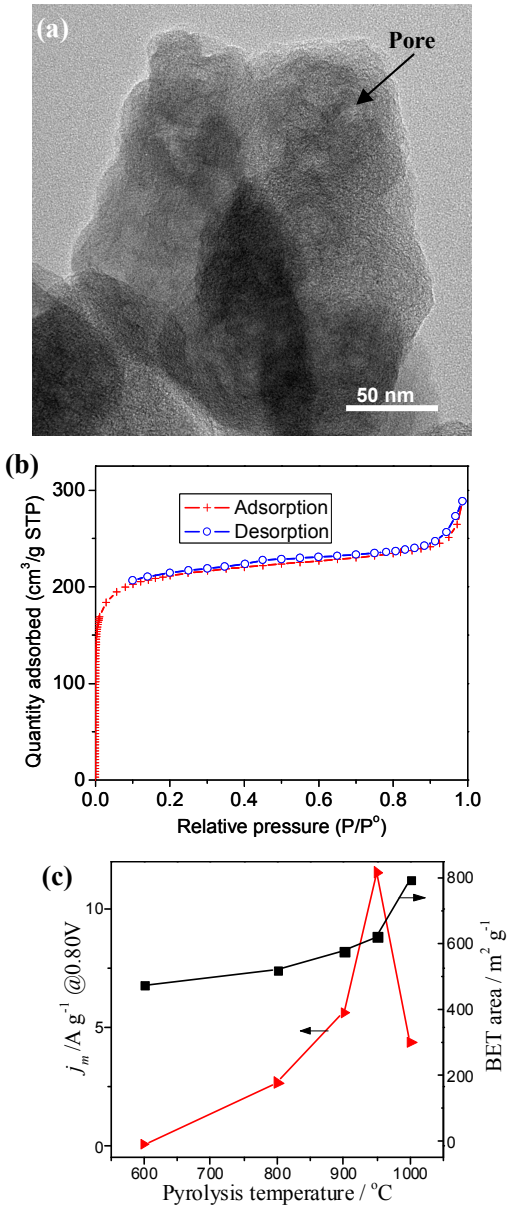

Figure S4 TEM image (**a**) and Ar adsorption/desorption isotherm (**b**) of P*m*PDA-FeN$_x$/C (950 ^{o}C) catalyst. (**c**) The dependence of ORR kinetic density (Left) and BET area (Right) on the pyrolysis temperature.

Figure S4a shows the TEM image of final P*m*PDA-FeN$_x$/C (950 ^{o}C) catalyst. No discernable crystalline species (high contrast) can be observed. The catalyst is made of carbon particles with the size ranging from 50~150 nm. Many porous structures can be seen. Argon adsorption/desorption isotherm analysis shows the catalyst has a BET surface area of 656 m^2 g^{-1}. Among them, micropore area is 498 m^2 g^{-1} and external surface area is 158 m^2 g^{-1} based on *t*-Plot analysis. So, the P*m*PDA-FeN$_x$/C is a micropore-type catalyst.

We found BET area of the catalysts increases with increasing pyrolysis temperature. However, at 1000 ^{o}C, although BET area is quite high (792 m^2 g^{-1}), the ORR activity greatly decreases to 4.4 A g^{-1}.

So, high BET area is not always a good criterion for high activity, and high density of active sites is essential. Excessively high temperature (e.g., 1000 ^{o}C) is not in favor of the formation of active sites.

8. Determination of ORR activity

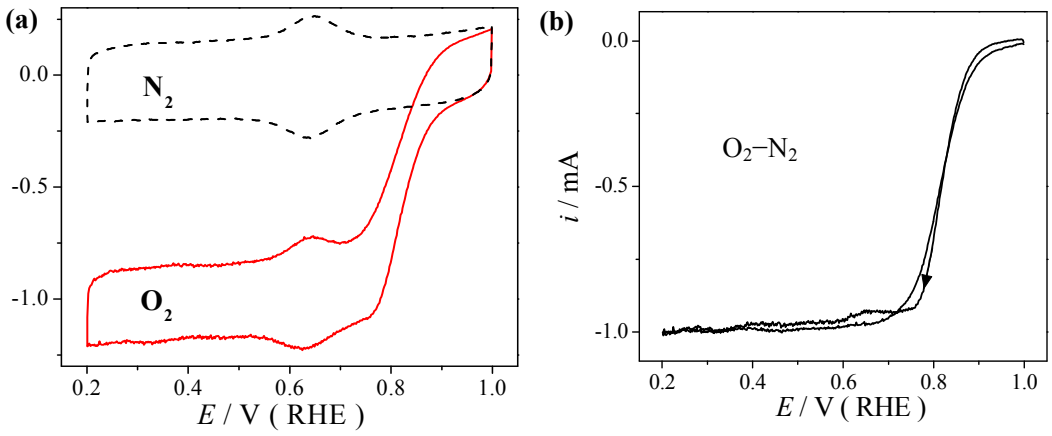

Figure S5 (**a**) Original polarization curves of P*m*PDA-FeN$_x$/C (950 ^{o}C) catalyst recorded in 0.1 M H_2SO_4 solution saturated with O_2 (red-solid line) and N_2 (black-dashed line). (**b**) Background-subtracted ORR polarization curve.

Figure S5a depicts the original polarization curves of P*m*PDA-FeN$_x$/C (950 ^{o}C) catalyst recorded in 0.1 M H_2SO_4 solution saturated with O_2 or N_2. Large capacitive current can be observed in the polarization curve recorded in N_2-saturated solution due to high specific surface area of the catalyst, and a couple of peaks at about 0.65 V are the redox of quinone/ hydroquinone, indicating the high oxygen content of the catalyst.

After the N_2-background (capacitive current) subtracting, the forward and backward of ORR polarization curves are overlapped (Figure S5b). In this study, only backward (negative) scan curve was displayed for clarity.

9. Comparison the ORR performance of different samples

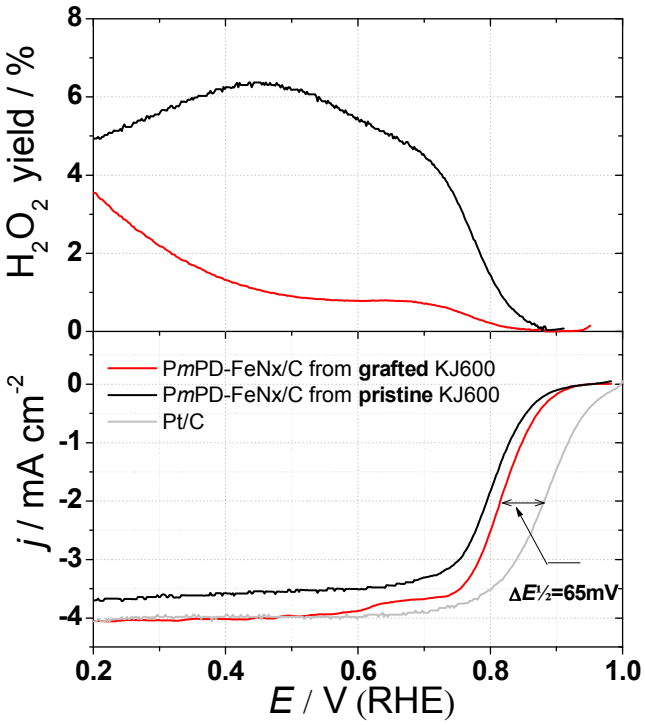

Figure S6 ORR polarization curves of P*m*PDA-FeN$_x$/C (950 ^{o}C) catalyst prepared from sulfophenyl-grafted KJ600 carbon black (red lines) and pristine KJ600 carbon black (black lines) in O_2-saturated 0.1 M H_2SO_4, as well as commercial Pt/C (20 wt%, JM) with a loading of 20 μg Pt cm^{-2} in O_2-saturated 0.1 M $HClO_4$. 900 rpm; 10 mV s^{-1}. To avoid the effect of anion specific adsorption (e.g., SO_4^{2-}) and surface oxide species, the ORR of Pt/C was tested in 0.1 M $HClO_4$, and positive-going scan was employed.

The ORR performance of P*m*PDA-FeN$_x$/C (950 ^{o}C) is less than that of Pt/C, and the half-wave potential gap was about 65 mV. If the P*m*PDA-FeN$_x$/C catalyst was prepared from pristine KJ600 carbon black without surface modification, the ORR mass activity was about 5.2 A g^{-1}, only about half of that (11.5 A g^{-1}) from sulfophenyl-grafted carbon black, and H_2O_2 yield was also very high.

10. Dependence of H_2O_2 yield on catalyst loading

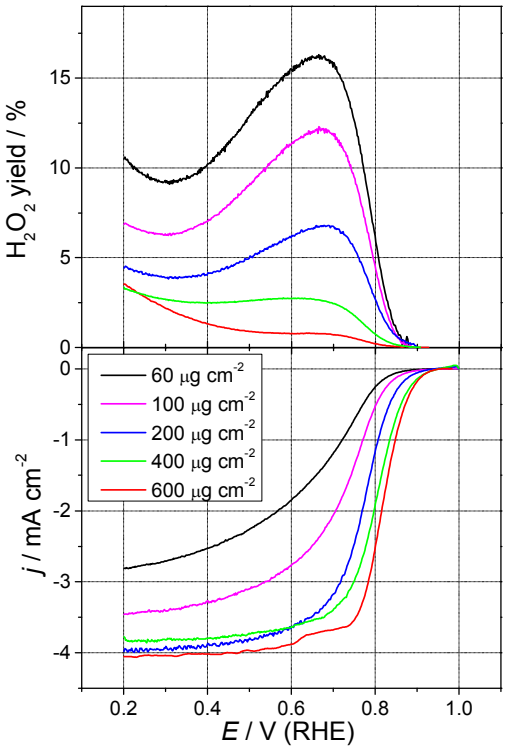

Figure S7. ORR polarization curves of P*m*PDA-FeN_x/C (950 ^oC) with different catalyst loading from 60 to 600 μg cm^{-2} on the GC disk electrode of the RRDE. 900 rpm; 10 mV s^{-1}.

Figure S7 illustrates the ORR current (bottom) and H_2O_2 yield (top) of P*m*PDA-FeN_x/C (950 ^oC) with different catalyst loading on the GC disk electrode of the RRDE. It is clear that H_2O_2 yield increases significantly with decreasing catalyst loading, indicating that indirect pathway (O_2 → H_2O_2 → H_2O) involves for ORR on the P*m*PDA-FeN_x/C.

11. XPS analysis of the P*m*PDA-FeN$_x$/C

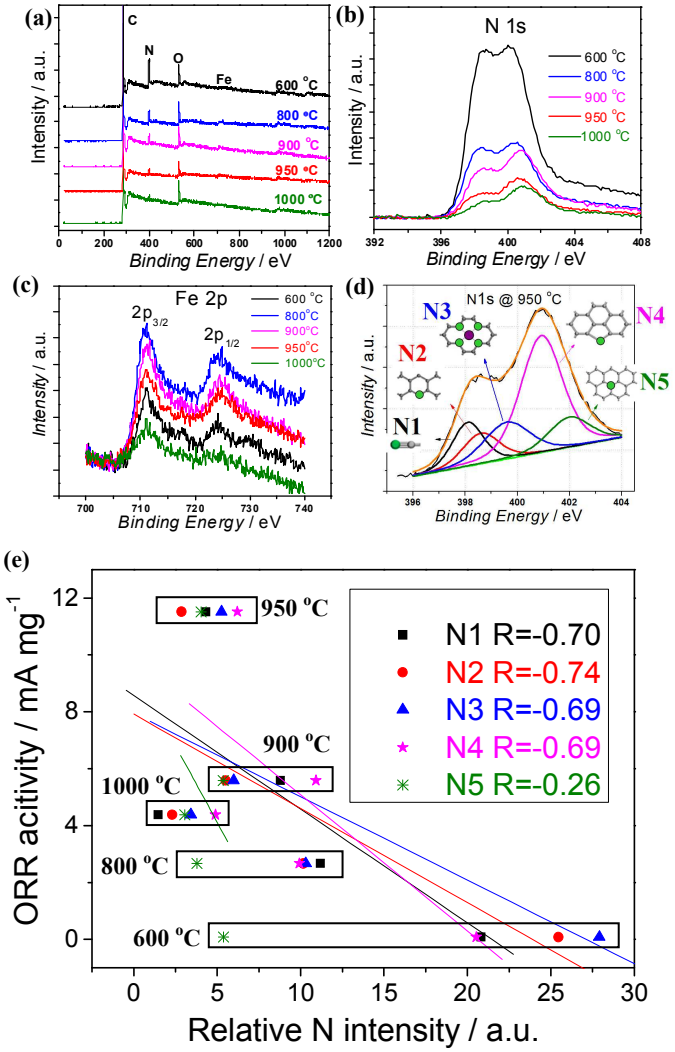

Figure S8. XPS of P*m*PDA-FeN$_x$/C catalyst prepared at different pyrolysis temperature. (a) survey spectra; (b) N 1s spectra; (c) Fe 2p spectra; (d) Deconvolution of N 1s spectrum for the sample prepared at 950 ^{o}C, according to the method proposed in Ref S2. The green cycle is nitrogen atom. (**e**) Poor correlation between the amounts of different N species and the ORR activity.

The P*m*PDA-FeN$_x$/C prepared at different pyrolysis temperature contain C, N, O, and Fe elements. As pyrolysis temperature increases, the N content decreases. Through peak deconvolution proposed in Ref S2, five N species can be discerned. The N1 to N5 species are cyano-N (-CN), pyridinic-N, pyrrolic-N, graphitic-N and Fe-N (e.g., FeN_4) as proposed by Ref S2. However, none of them can directly correlate with the ORR activity, and the relevant coefficients (R) were even negative values. The weight percents of N and Fe for the PmPDA-FeNx/C (950 ^{o}C) were 4.2 % and 0.74 %, determined by CHNS elemental analysis and ICP-OES, respectively.

12. Effect of SCN^- on the ORR activity of P*m*PDA-FeN_x/C

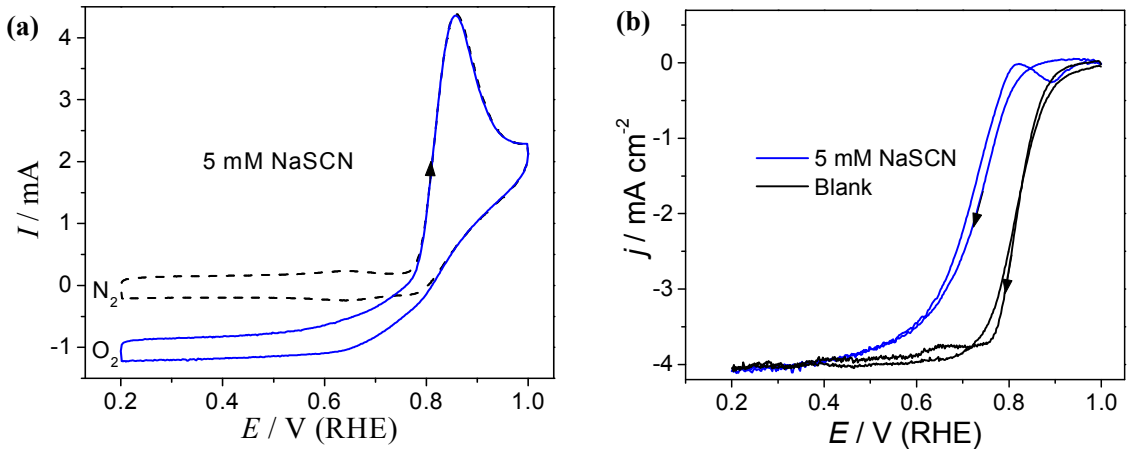

Figure S9 (**a**) Original polarization curves of P*m*PDA-FeN_x/C (950 ^oC) catalyst recorded in 0.1 M H_2SO_4 + 5 mM NaSCN solution saturated with O_2 (blue-solid line) and N_2 (black-dashed line). (**b**) Background-subtracted ORR polarization curve recorded in 0.1 M H_2SO_4 + 5 mM NaSCN and blank (0.1 M H_2SO_4) solution.

In the N_2-saturated solution, SCN^- ion can be oxidized at $E > 0.77$ V in the forward scan, yielding a peak at 0.87 V. In the O_2-saturated solution, SCN^- ion shows the similar electrochemical oxidation behavior besides ORR. After the N_2 background subtracting, the forward and backward ORR polarization curves are nearly overlapped in 0.1 M H_2SO_4 + 5 mM NaSCN solution (Figure S9b). In comparison with the ORR polarization curves recorded in the blank solution (i.e., 0.1 M H_2SO_4), it is clear that SCN^- ion can greatly suppress the ORR activity of P*m*PDA-FeN_x/C.

13. Effect of SO_2 and H_2S on the ORR activity of P*m*PDA-FeN_x/C

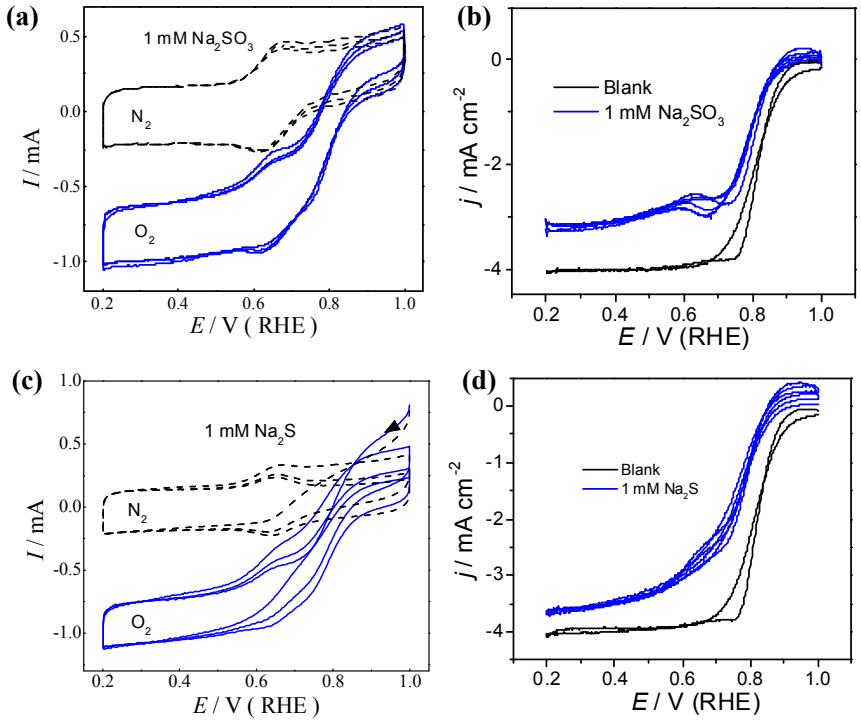

Figure S10 Original polarization curves of P*m*PDA-FeN_x/C (950 ^oC) catalyst recorded in 0.1 M H_2SO_4 + 1 mM Na_2SO_3 (**a**) and 0.1 M H_2SO_4 + 1 mM Na_2S (**c**) saturated with O_2 and N_2. (**b, d**) Comparison of background-subtracted ORR polarization curves with and without the additive of 1 mM Na_2SO_3 and 1 mM Na_2S.

Figure S10 demonstrates the effect of Na_2SO_3 and Na_2S (real forms are SO_2/H_2SO_3 and H_2S in acidic solution, respectively) on the ORR activity of P*m*PDA-FeN_x/C catalyst. In the original polarization curves (Figure S10a and S10c), it can be seen that both SO_2 and H_2S can be oxidized at potential higher than ca. 0.6 V in both N_2- and O_2-saturated solution. The oxidation current gradually decreases with increasing cycling numbers due to the decrease of SO_2 and H_2S concentrations by N_2 or O_2 bubbling. After the N_2 background subtracting, the forward and backward ORR polarization curves are nearly overlapped for solutions containing both SO_2 and H_2S (Figure S10b and S10d). In comparison with the ORR polarization curves recorded in the blank solution (i.e., 0.1 M H_2SO_4), it is clear that SO_2 and H_2S can greatly inhibit the ORR activity of P*m*PDA-FeN_x/C, and the polarized potentials at 2 mA cm^{-2} are decreased by about 40 and 70 mV, respectively. As for SO_2, even the diffusion-limited current was also decreased remarkably.

14. Effect of SeO_2 and TeO_3^{2-} on the ORR activity of P*m*PDA-FeN_x/C

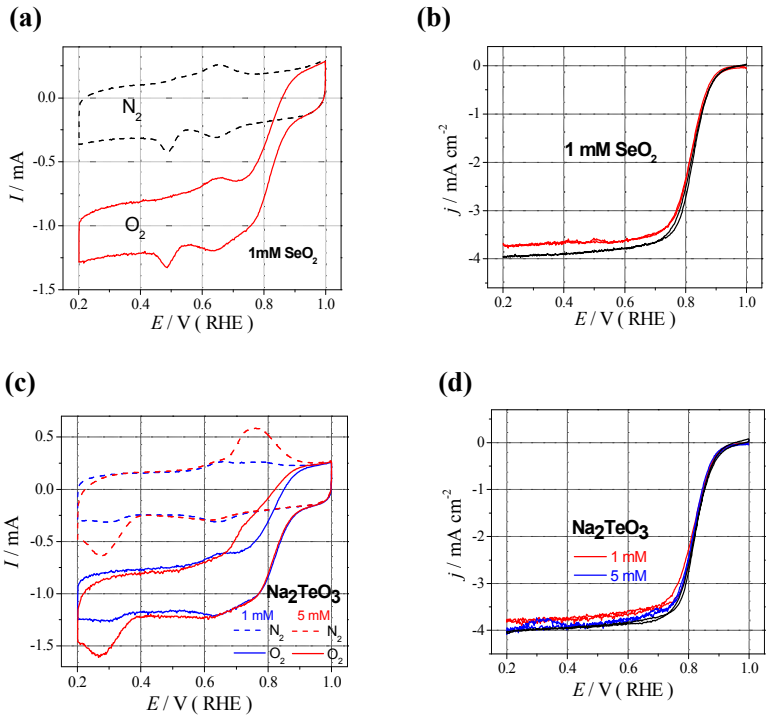

Figure S11 Original polarization curves of P*m*PDA-FeN_x/C (950 ^oC) catalyst recorded in 0.1 M H_2SO_4 solution containing 1 mM SeO_2 (**a**), and 1 and 5 mM Na_2TeO_3 (**c**) saturated with O_2 and N_2. Comparison of background-subtracted ORR polarization curves with and without the additives of SeO_2 and Na_2TeO_3 (**b, d**).

SeO_2 shows a weak reduction peak at about 0.5 V, and TeO_3^{2-} shows a reduction peak at 0.26 V, and an oxidation peak at 0.76 V. After the N_2 background subtracting, the forward and backward ORR polarization curves are nearly overlapped for both solutions containing SeO_2 and TeO_3^{2-} (Figure S11b and S11d), and also overlapped with the polarization curves recorded in blank solution. Clearly, both SeO_2 and TeO_3^{2-} can not influence the ORR activity of P*m*PDA-FeN_x/C.

15. Effect of SCN^-, SO_2 and H_2S on the ORR activity of Pt electrode

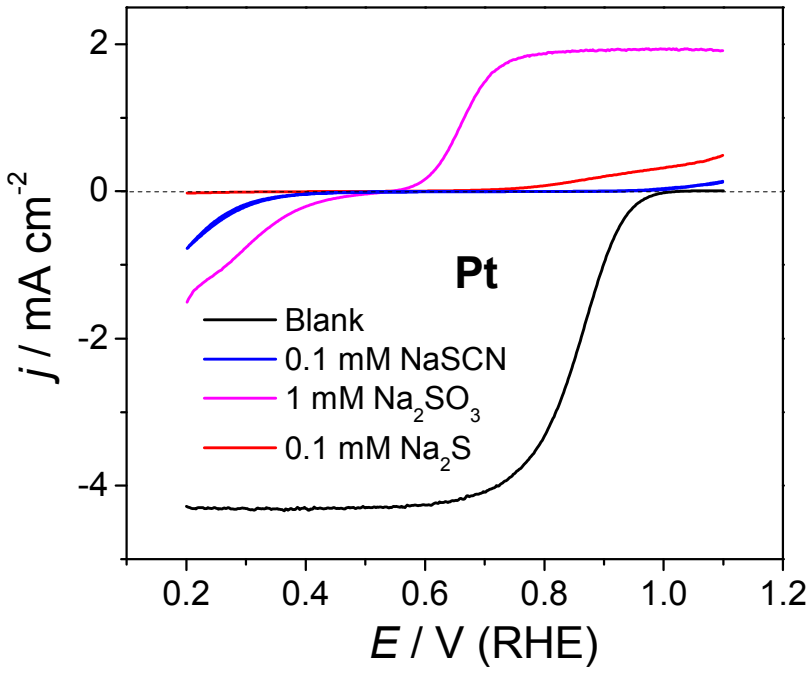

Figure S12 ORR polarization curves of a bulk Pt electrode recorded in 0.1 M H_2SO_4 solution and 0.1 M H_2SO_4 containing 0.1 mM NaSCN, 1 mM Na_2SO_3, and 0.1 mM Na_2S.

As expectation, low valence state sulfur-containing species can seriously poison the Pt electrode for ORR. For example, 0.1 mM of SCN^- or H_2S can completely suppress the ORR activity.

15. Effect of SCN^- concentration on the ORR activity of PmPDA-FeNx/C

As expectation, increasing the contaminant concentration will decrease the ORR activity of PmPDA-FeN_x/C. As shown in Figure S13, the potential was held at 0.75 V, and the SCN^- ion concentration was increased from zero to 5 mM by a step of 1 mM. The ORR activity can be greatly decreased by adding of the initial 1 mM SCN^- ion, and gradually trends to stable value when SCN^- increases to 5 mM.

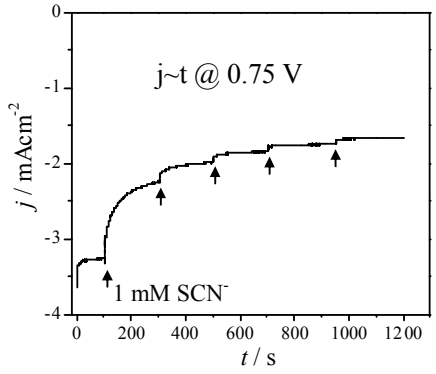

Figure S13. Effect of SCN^- concentration on the ORR activity of PmPDA-FeN_x/C.

References

[S1] Zhou, Z. Y.; Kang, X. W.; Song, Y.; Chen, S. W. *J. Phys. Chem. C* **2012**, 116, 10592-10598.

[S2] Artyushkova, K.; Kiefer, B.; Halevi, B.; Knop-Gericke, A.; Schlogl, R.; Atanassov, P. *Chem. Commun.* **2013**, 49, 2539-2541.

Full author list of Ref 1 in Main text

(1) Borup, R.; Meyers, J.; Pivovar, B.; Kim, Y. S.; Mukundan, R.; Garland, N.; Myers, D.; Wilson, M.; Garzon, F.; Wood, D.; Zelenay, P.; More, K.; Stroh, K.; Zawodzinski, T.; Boncella, J.; McGrath, J. E.; Inaba, M.; Miyatake, K.; Hori, M.; Ota, K.; Ogumi, Z.; Miyata, S.; Nishikata, A.; Siroma, Z.; Uchimoto, Y.; Yasuda, K.; Kimijima, K. i.; Iwashita, N. *Chem. Rev*. **2007**, 107, 3904-3951.